JMES The International Journal of
Mechanical Engineering and Sciences
https://journal.its.ac.id/index.php/jmes/index
e-ISSN 2580-7471

Numerical Investigation of Impeller Leading-edge Profiling on Vortex Suppression and Performance Enhancement in a Pump-as-turbine

Fadhlurrahman, Sutardi*

Department of Mechanical Engineering, ITS, Sukolilo Surabaya 60111, Indonesia

Received: 10 June 2026, Revised: 24 June 2026, Accepted: 25 June 2026

Abstract

Centrifugal pumps operating as turbines (PAT) offer a cost-effective solution for micro-hydro power plants. However, their hydraulic performance is compromised by flow separation at the impeller's outer diameter. This study conducted a transient numerical analysis to evaluate the hydrodynamic effects of modifying sharp blade edges into rounded profiles. The mesh structure setup, consisting of Poly-Hexcore with a k–ω turbulence model using Computational Fluid Dynamics (CFD) in ANSYS Fluent with the Meshing solver, was validated based on experimental data and applied across a wide operational range ($27.75 \leq Q \leq 65.0$ L/s). Performance characteristic analysis shows that rounded blades significantly improve energy extraction. At the PAT best efficiency point (BEP), efficiency increased from 65.46% to 68.79%, and the mechanical shaft power output increased by 29.96%. Physical evaluation of pressure contours and velocity flow-line topologies validated these benefits. An impeller with sharp blades causes severe flow separation and generates turbulent vortices that obstruct flow on the suction side of the blades. Conversely, an impeller with rounded blades successfully suppresses vortex formation and maintains a flow topology that adheres to the blade curvature, ensuring uniform momentum transfer to the rotor.

Keywords: Pump as Turbine, Computational Fluid Dynamics, Impeller Rounding, Micro-Hydropower.

1. Introduction

Global shifts toward sustainable energy infrastructure are leading to small-scale renewable energy systems that serve local areas. In this context, micro-hydro power plants have emerged as a highly suitable solution for supporting local rural power grids [1, 2]. However, from an economic standpoint, micro-hydro power plants face significant barriers due to the high costs associated with procuring conventional turbines, such as Francis and Pelton turbines [3]. The use of centrifugal pumps operated as turbines can be a solution that offers low procurement and operational costs as well as a simple operating system [4].

Although economically superior, the performance of the PAT is not optimal because the fluid is forced to pass through a geometrically suboptimal path [5, 6]. The most critical loss occurs at the outer diameter of the impeller, which serves as the turbine inlet [7]. The fluid enters by striking the sharp trailing edge (now the leading edge) of the backward-curved vane. This results in boundary layer separations, the formation of wake regions, numerous vortices, and the dissipation of kinetic energy [8, 9]. Specifically, Ismail *et al.* [8] demonstrated wake reduction using steady-state velocity vector visualizations, while Tchada *et al.* [9] quantified shock and swirling losses under part-load conditions. However, both studies relied on steady-state frameworks and noted diminishing returns at higher flow rates. Consequently, efficiency is significantly reduced, and the operational range of the PAT is narrowed.

To reduce hydrodynamic losses, modifications to the impeller and casing of a standard centrifugal pump are necessary. Geometric modifications to the volute can improve the performance characteristics of the pump. Parameters based on the casing radius indicate changes in axial load during rotor–stator interaction, which previously exhibited mismatch [10]. Additionally, modifications to the impeller, specifically rounding the sharp leading edges of the impeller blades, can reduce flow separation, thus increasing output power at nominal speed [11, 12]. Changes to the leading-edge profile can also shift the best efficiency point (BEP) of the PAT. However, no prior study has systematically examined the transient vortex dynamics caused by leading-edge rounding in PAT impellers. Specifically, the internal flow kinematics and vortex suppression mechanisms under off-design conditions remain unexplored.

Therefore, the primary objective of this study is to explain the transient hydrodynamic mechanisms resulting from rounding the leading edges of the impeller blades. PAT design modeling was performed and numerically analyzed using Computational Fluid Dynamics (CFD) in ANSYS Fluent with the Meshing solver [13, 14]. Performance analysis of the PAT was conducted by examining changes

*Corresponding author. Email: sutardi@me.its.ac.id, phone: +62 81232223645

in head, power, and overall efficiency at the turbine's operating point. An examination of the physical characteristics occurring when the leading edge of the impeller blades is rounded was performed by analyzing the contours of pressure, velocity, and fluid streamlines.

2. Numerical Methods and Validation

2.1. Geometric Model and Blade Profiling

The geometric configuration of the PAT consists of a single-stage centrifugal pump constructed based on the experimental prototype described by [10]. The computational domain comprises an inlet pipe, a volute casing, and a rotating impeller. The impeller has 6 backward-curved blades with an outer diameter of 260 mm, an impeller eye diameter of 120 mm, and a uniform blade thickness of 3 mm. The blade tips were modified from sharp to rounded, with a rounding radius equal to half the blade thickness [12]. Figure 1 shows the shapes of the impeller with sharp blades and the impeller with rounded blades.

2.2. Governing Equations

The internal flow of the PAT is considered an incompressible, fully turbulent, and transient fluid domain. The numerical solution is governed by the Unsteady Reynolds-Averaged Navier-Stokes (URANS) equations, which are solved to determine the flow field characteristics. The continuity and momentum equations are expressed in Eq. 1 and Eq. 2 [15].

Where $\overline{u}_i$ and $\overline{u}_j$ represent the time-averaged velocity components, $\overline{p}$ is the time-averaged pressure, ρ is the fluid density, and ν is the kinematic viscosity. The term $-\rho\overline{u_i'u_j'}$ represents the Reynolds stress tensor, which captures the effects of turbulent fluctuations on the mean flow. To close the system of equations and model the Reynolds stresses, the two-equation k–ω Shear Stress Transport (SST) turbulence model was selected due to its robust capability in predicting flow separation under adverse pressure gradients typical in turbomachinery [16].

2.3. Numerical Setup

The computational domain was set up using the Poly-Hexcore topology in ANSYS Fluent with the Meshing solver. Local mesh size was controlled using curvature and proximity controls applied to the impeller and volute walls. Subsequently, a boundary layer satisfying the y^+ criterion was applied starting from the first layer adjacent to the impeller. The mesh was generated using a Poly-Hexcore topology with a growth rate of 1.2 and a boundary layer consisting of 15 layers.

$$\frac{\partial \bar{u}_i}{\partial x_i} = 0 \tag{1}$$

$$\frac{\partial \bar{u}_i}{\partial t} + \bar{u}_j \frac{\partial \bar{u}_i}{\partial x_j} = -\frac{1}{\rho}\frac{\partial \bar{p}}{\partial x_i} + \nu \frac{\partial^2 \bar{u}_i}{\partial x_j \partial x_j} - \frac{\partial}{\partial x_j}\left(\overline{u_i'u_j'}\right) \tag{2}$$

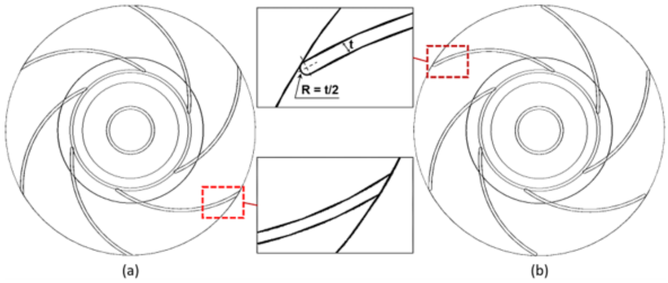

Figure 1. Comparison of the impeller geometric profiles for (a) the original sharp-edge design and (b) the modified rounded-edge design (R = t/2).

The average orthogonal quality and skewness values served as key factors for evaluating mesh quality prior to the computation [17]. Figure 2 shows the meshed domain with the Poly-Hexcore topology.

2.4. Grid Independence Test

A grid independence study was conducted to ensure the accuracy of the computations by evaluating an optimal balance between numerical accuracy and computational hardware efficiency [18]. The grid independence test was performed at a rotational speed of 1450 rpm and a flow rate of 33.50 L/s. Head and efficiency in the PAT were the factors examined in the grid independence test shown in Figure 3. With a total of 3,433,373 cells across the entire impeller-and-volute domain, a balance was achieved between computational accuracy and computational cost. The relative deviations were negligible at 0.82% for head and 0.15% for efficiency. Interestingly, with a larger number of cells (4.4×10^6), there was a sharp decrease in head of 4.27% and an increase in efficiency of up to 6.30%. This phenomenon is known as a characteristic of the Unsteady Reynolds-Averaged Navier–Stokes (URANS) method when the mesh scale approaches the energy-containing scales of turbulence. Refining the mesh beyond a certain threshold can lead to an overlap between the modeled and resolved turbulent scales. Under these conditions, the required spectral gap for the URANS formulation is compromised that leading to numerical inconsistencies. The solver begins to resolve transient scales that the k–ω model is intended to statistically average, this can lead to overestimation of flow characteristics [19]. When the cells are too fine in the boundary layer, the dissipation rate (ω) can become singular, which disrupts the stability of the solver [20].

2.5. Experimental Validation of the Numerical Model

To evaluate the quantitative performance of a PAT system (head, torque, and efficiency), calculations based on numerical results are required. Torque (T) is the magnitude of the rotational force exerted by the velocity magnitude (ω) from fluid on the impeller blades. This torque value determines the amount of mechanical shaft power (P_m) generated by the turbine using Eq. 3 [21]. Meanwhile, head (H) represents the total hydraulic energy

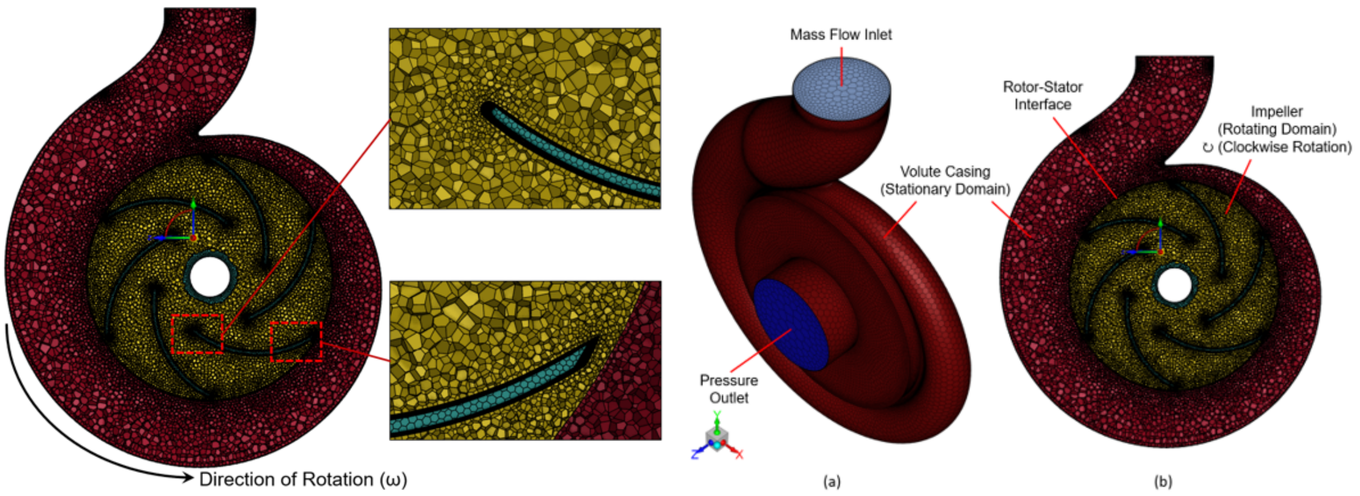

Figure 2. 3D computational Poly-Hexcore mesh illustrating (a) boundary conditions, axis, and fluid domain; and (b) Spatial discretization of the PAT computational domain

extracted by the PAT from the fluid, corresponding to the total pressure difference between the suction (P_s) and discharge (P_d) sides of the PAT, which can be calculated using Eq. 4 [21]. The magnitude of the generated head will determine the magnitude of the hydraulic power (P_h) of the fluid entering the turbine using Eq. 5 [21]. The comparison of these two powers (mechanical and hydraulic) will determine the overall efficiency (η) of the turbine using Eq. 6 [21].

Validation was performed to ensure the accuracy of the calculations. The results of the numerical calculations for the basic impeller without rounding were compared with experimental data provided by [10]. Validation was conducted across the entire operational range of the PAT. The comparison results for head (H), power (P), and efficiency (η) are presented in Table 1. The numerical computations show strong agreement with the experimental data. The average relative errors across the entire operational range were 9.23% for head, 6.41% for power, and 2.60% for efficiency. At the point of best PAT efficiency, the numerical calculation deviated by only 2.54%. The main discrepancy, particularly regarding excessively high head values outside the design range, is a characteristic of the URANS turbine simulation. This deviation is caused by the neglect of mechanical friction (bearing and seal losses)

$$P_{\mathrm{m}} = T\omega \tag{3}$$

$$H = \frac{P_{\mathrm{s}} - P_{\mathrm{d}}}{\rho g} \tag{4}$$

$$P_{\mathrm{h}} = \dot{m} g H \tag{5}$$

$$\eta = \frac{P_{\mathrm{m}}}{P_{\mathrm{h}}} \tag{6}$$

as well as leakage flow from the wear ring [19]. Given that the assumptions are merely standard modeling practices, the numerical calculations performed are considered highly reliable for conducting comparative studies.

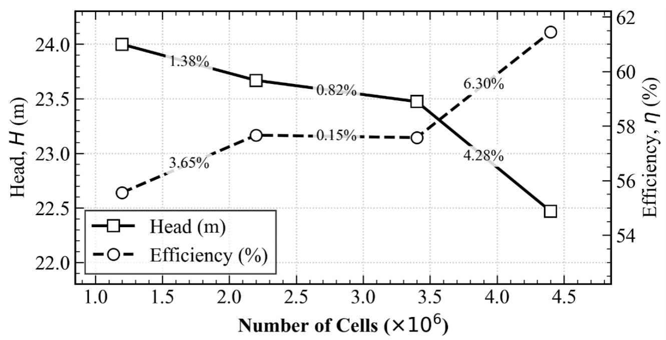

Figure 3. Grid independence analysis evaluating head (H) and efficiency (η) convergence.

3. Results and Discussion

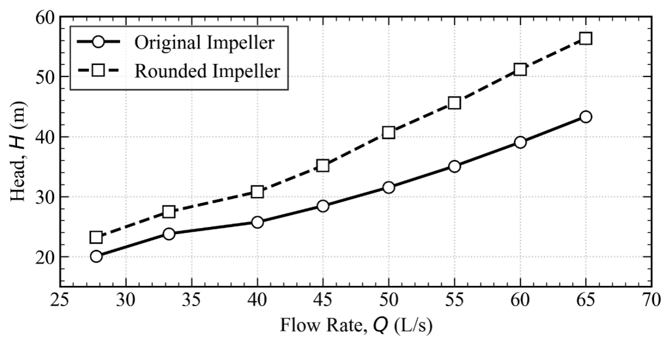

Figure 4. Comparison of head-flow rate (H-Q) characteristics between the original and rounded impellers operating in turbine mode.

Table 1. Numerical validation against experimental data [10] for the baseline impeller.

Q	Head, H (m)			Power, P (kW)			Efficiency, η (%)		
(L/s)	Exp. [10]	Num.	Error (%)	Exp. [10]	Num.	Error (%)	Exp. [10]	Num.	Error (%)
27.75	18.43	20.08	8.96	2.49	2.91	16.93	49.79	53.39	7.23
33.50	21.12	23.80	12.68	4.07	4.51	10.79	58.71	57.67	-1.77
40.00	24.04	25.73	7.03	5.96	6.38	6.97	63.31	63.30	-0.01
45.00	27.11	28.44	4.90	8.02	8.20	2.21	67.17	65.46	-2.54
50.00	30.29	31.53	4.10	10.40	9.98	-4.08	70.11	64.68	-7.75
55.00	32.15	35.06	9.05	11.47	11.57	0.85	66.28	61.29	-7.53
60.00	35.22	39.03	10.82	12.85	13.62	6.03	62.12	59.42	-4.35
65.00	37.24	43.31	16.30	13.16	14.68	11.57	55.53	53.26	-4.10

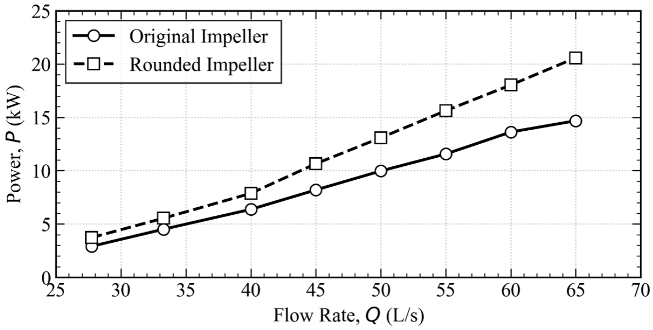

Figure 5. Comparison of power-flow rate (P-Q) characteristics between the original and rounded impellers operating in turbine mode.

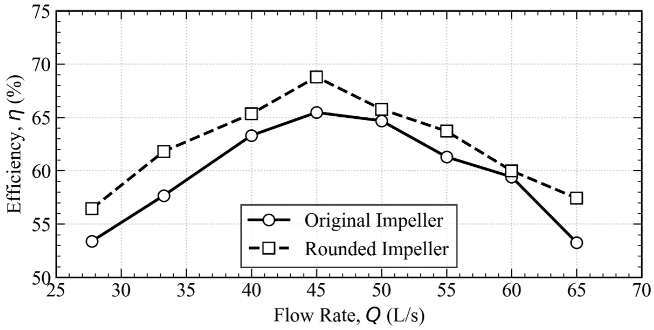

Figure 6. Comparison of efficiency-flow rate (η-Q) characteristics between the original and rounded impellers operating in turbine mode.

3.1. PAT Performance Characteristics

Figure 4 shows the H–Q characteristics for the original impeller with sharp blades and the impeller with rounded blades. In both configurations, the head increases as the flow rate increases. Most importantly, rounding the outer edges of the impeller blades has a positive effect, as indicated by an upward shift in the curve across the entire H–Q curve. At the original flow rate ($Q = 33.50$ L/s), the head increased by 3.65 m. However, at the increased flow rate ($Q = 65.0$ L/s), the maximum deviation reached 13.03 m.

This deviation trend indicates that even the rounding of the outer impeller blades alters the rotor-stator incidence angle. Impellers with sharp blades often experience severe flow separation and trigger the formation of stagnant flow regions. By rounding the outer blades of the impeller, the boundary layer remains attached over a relatively wide range of angles [9]. This suppresses the occurrence of turbulent flow by forcing the fluid to follow the curved lines of the rounded blades. Consequently, the flow shear factor is minimized, allowing the impeller to extract greater hydraulic energy from the fluid.

Figure 5 shows the P–Q characteristics with mechanical shaft power as a function of fluid flow rate. As the head value increases, the impeller with rounded blades produces significantly higher mechanical power at all measured flow rates. Under oversized flow conditions ($Q = 65$ L/s), the power output increases from 14.68 kW for the original blades to 20.58 kW for the rounded blades. In the original pump, the best efficiency point (BEP) was at a flow rate of 33.50 L/s. However, numerical results indicate that when operated as a turbine, the BEP shifts to a higher flow rate of 45.0 L/s. This shift occurs because higher flow rates and head are required in turbine mode to compensate for losses and achieve the optimal speed triangle.

As shown in Figure 6, the BEP of the PAT with rounded blades increases efficiency from 65.46% for the original sharp blades to 68.79% for the rounded blades. Rounding the blades maintains efficiency above 60% over a wider range of operational flow rates. This confirms that rounding the blades not only increases power output but also minimizes thermodynamic and hydraulic losses, particularly under off-design conditions [12].

3.2. Internal Flow Characteristics

3.2.1. Pressure Distributions

Figure 7 shows the pressure contours for an impeller with rounded edges across the entire operating range. In turbine mode, the volute casing acts as a high-pressure manifold that distributes the fluid radially into the impeller. Figure 8 shows the pressure contours of the original

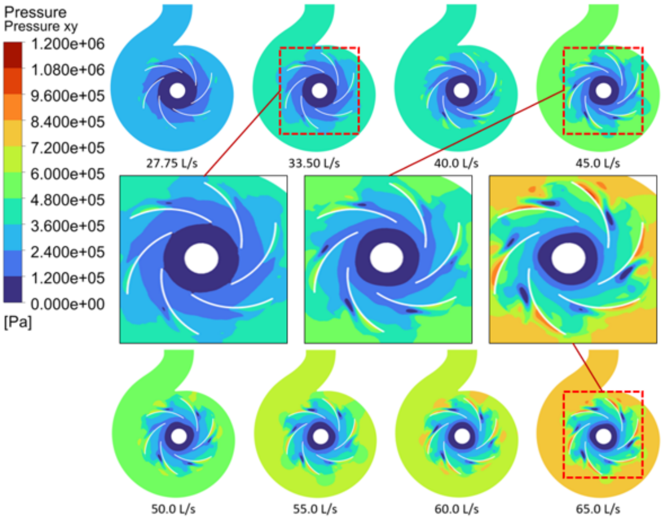

Figure 7. Pressure distributions at the mid-span plane of the modified rounded-edge impeller.

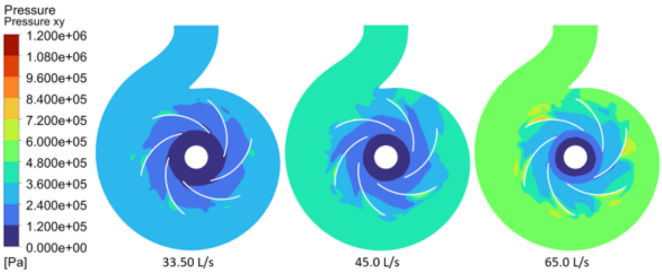

Figure 8. Pressure distributions at the mid-span plane of the original sharp-edge impeller.

impeller with sharp edges for comparison at a flow rate of 33.5 L/s; the best efficiency point (PAT) at 45.0 L/s; and an excess flow rate of 65.0 L/s.

At a flow rate of 33.5 L/s, there was no significant difference in pressure distribution between the original impeller and the rounded impeller. The pressure gradients formed were generally uniform for both impellers, but a more symmetrical pressure distribution began to emerge for the rounded impeller. This indicates that no significant flow separation occurred in the rounded impeller. At the flow rate corresponding to the BEP ($Q = 45.0$ L/s), a clear difference is observed in the rounded impeller, marked by the increasingly symmetrical pressure distribution occurring from the outer diameter toward the impeller's eye. In contrast, for the original impeller with sharp blades, flow separation occurs distinctly due to fluid acceleration, resulting in sharp geometric discontinuities. The most striking difference occurs under overflow conditions ($Q = 65.0$ L/s). In the original impeller, flow separation occurs completely from the blade surface due to local pressure that triggers hydrodynamic drag. This causes turbulent vortices and the failure of momentum transfer to the rotor.

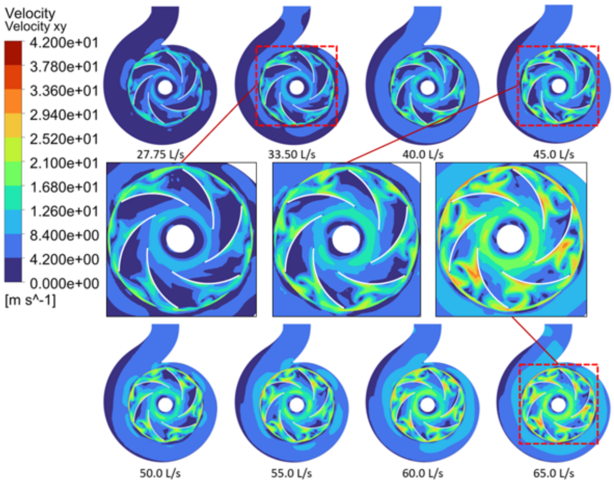

Figure 9. Velocity distributions at the mid-span plane of the modified rounded-edge impeller.

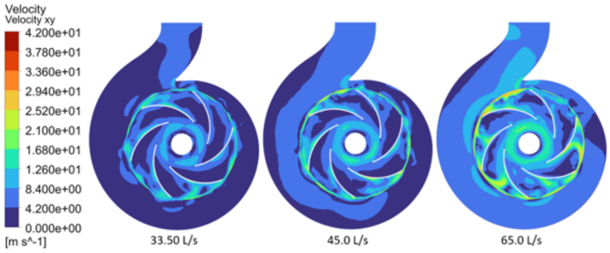

Figure 10. Velocity distributions at the mid-span plane of the original sharp-edge impeller.

3.2.2. Velocity Distributions

Figure 9 shows the velocity contours for the rounded impeller across the entire range of operational flow rates. In turbine mode, the volute acts as a nozzle that accelerates the fluid flow before it enters the impeller. This condition is compared to the sharp velocity contours of the original impeller at a flow rate of 33.5 L/s; the best efficiency point (PAT) at 45.0 L/s; and an overshoot flow rate of 65.0 L/s, as shown in Figure 10.

At a flow rate of 33.5 L/s, the relative velocity is low for both the original and rounded impellers. The flow moves through the blades with minimal flow separation, as indicated by nearly identical power and efficiency values. As the flow rate increases to the BEP ($Q = 45.0$ L/s), the geometric effects of the impeller edges begin to become apparent. The impeller with sharp blades exhibits significant stagnation zones with severe velocity gradients at the blade edges. The resulting flow is unable to overcome the discontinuities of the sharp-bladed impeller and forms a low-velocity wake along the suction side of the blades. This effectively reduces the functional cross-sectional area and forces the fluid to accelerate unevenly. In contrast, the impeller with rounded blades exhibits a uniform velocity distribution. The rounded blade tips successfully guide the fluid along the curved path of the blades, suppressing boundary layer separation, and nearly

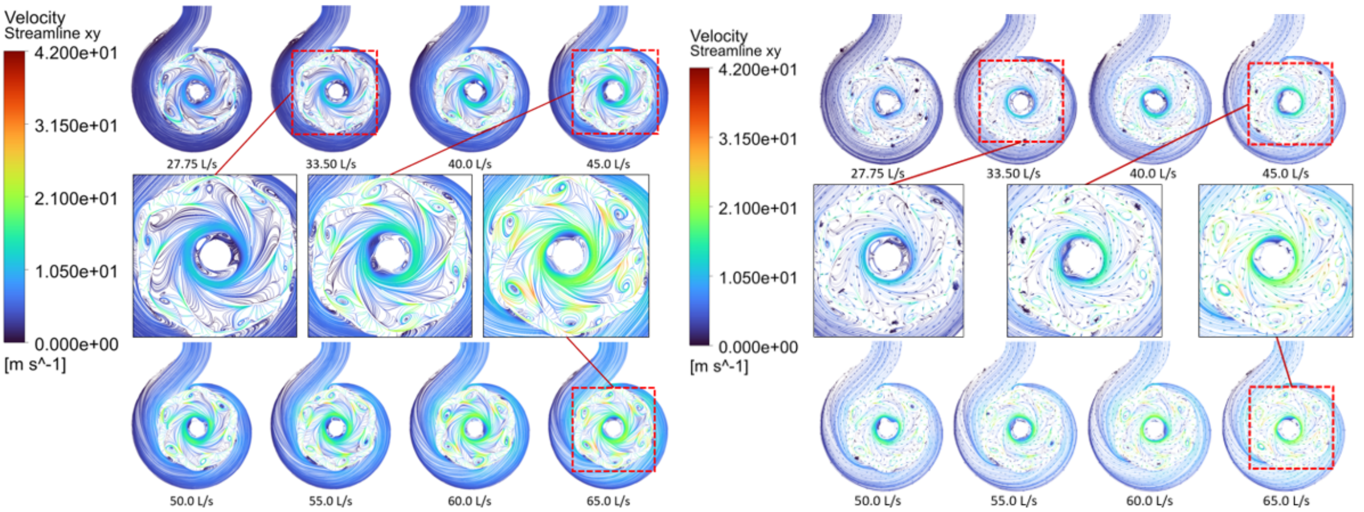

Figure 11. Velocity streamlines distributions at the mid-span plane of the modified rounded-edge impeller.

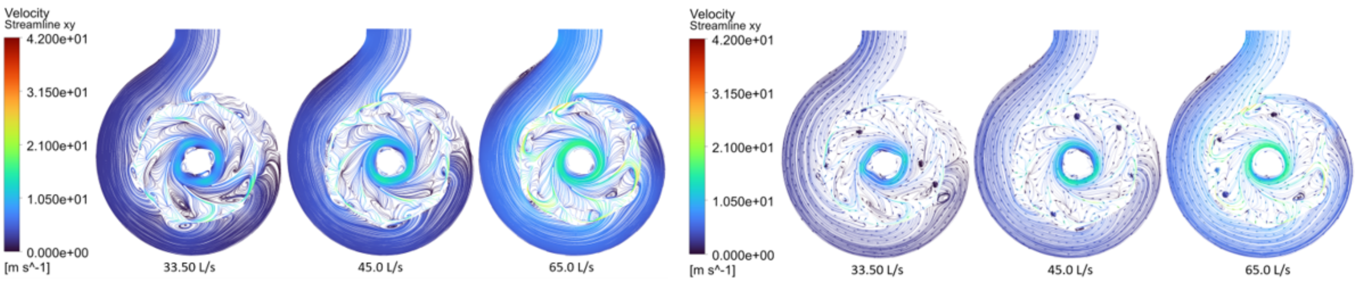

Figure 12. Velocity streamlines distributions at the mid-span plane of the original sharp-edge impeller.

eliminating residual flow. These conditions allow the turbine to generate greater hydraulic energy compared to the original impeller. At excessive flow rates ($Q = 65.0$ L/s), the original impeller experiences chaotic flow separation, and low-velocity flow trails dominate the blade channels, causing severe hydrodynamic blockage and energy loss. The impeller with rounded blades is able to limit the extent of the low-velocity flow traces, although it cannot completely prevent flow separation [22]. The main flow remains more uniform compared to the original impeller.

3.2.3. Velocity Streamlines Distributions

Velocity streamlines are used to reveal the topological structure of the flow by observing two-dimensional streamlines in the PAT mid-plane. Figure 11 shows the flow line topology on the rounded impeller for each operational flow rate compared to the original impeller in Figure 11 for a flow rate of 33.5 L/s; the PAT's best efficiency point at 45.0 L/s; and an excess flow rate of 65.0 L/s.

At a flow rate of 33.5 L/s, the relative velocity is low, yet flow separation has already occurred at the impeller's sharp angles. The recirculation zone (vorticity) clearly dominates most of the flow at the blades. The fluid becomes trapped in a rotating structure and dissipates kinetic energy there rather than transferring it to the impeller shaft. At the BEP ($Q = 45.0$ L/s), flow momentum increases and exacerbates flow separation. In the original impeller, the resulting vortices are larger, trapping fluid and narrowing the effective cross-sectional area of the channel. Consequently, high shear stress is generated, and the fluid experiences significant irreversible losses; this can be seen in the light blue line passing through the dark purple vortices. In contrast, with the impeller featuring rounded blades, flow separation is effectively suppressed [23]. The flow remains attached to the blade surface, and any vortices that form are immediately compressed, with their volume gradually decreasing. This flow topology ensures that fluid momentum is evenly distributed across the impeller blades, thereby enhancing efficiency. When excessive flow rate ($Q = 65.0$ L/s) occurs, the large volume of fluid cannot be accommodated by any blade profile and flow separation occurs. However, the fluid in the original impeller experiences severe blockage, and the resulting vortices completely fill the blade channel area. An impeller with rounded blades can maintain a bound flow and prevent flow separation from occurring across the blade gaps, thereby preserving the generated momentum [24].

To further evaluate the energy dissipation characteristics of the modified PAT, both the turbulent kinetic energy (TKE) and velocity swirling strength were analyzed under a constant available head condition, which closely mimics real-world micro-hydro site constraints [25]. When normalized to a constant head drop of approximately 35 meters, the original sharp-edge impeller required a substantially higher flow rate of 55.0 L/s, generating a volume-averaged TKE of 6.319 J/kg and a swirling strength of 290.26 s^{-1}. Conversely, the rounded impeller achieved the equivalent head utilizing only 45.0 L/s, yielding a reduced TKE of 5.734 J/kg and a lower swirling strength of 261.83 s^{-1}. Simultaneously, this 9.26% reduction in overall turbulent energy dissipation and 9.79% reduction in chaotic vortex intensity clearly demonstrate that under equivalent site conditions, the rounded leading-edge profile successfully mitigates hydrodynamic blockage. By suppressing these local vortices, the modified design preserves fluid momentum, allowing a greater fraction of the available hydraulic energy to be converted into mechanical shaft power.

4. Conclusions

This study successfully revealed the transient hydrodynamic mechanisms underlying how the geometric shape of impeller blades affects the performance of a centrifugal pump operating as a turbine. Numerical analysis shows that rounding the sharp edges of the impeller's outer-diameter blades can optimize internal flow kinematics. Rounded blades suppress severe vortices in the impeller's suction-side channel and reduce the hydrodynamic blockage that occurs in impellers with sharp blades. When evaluated under a constant 35-meter head, the optimized design successfully mitigates hydrodynamic blockage, generating a 9.26% reduction in turbulent kinetic energy dissipation and a 9.79% decrease in localized vortex intensity. These combined kinetic improvements directly manifest as a 3.3% increase in hydraulic efficiency at the best efficiency point (BEP), coupled with a 29.96% improvement in shaft power output.

Practically, a highly cost-effective design that is easily applicable to standard centrifugal pumps. The modifications also expand the stable operational range for micro-hydro power systems. Although this study has successfully solved the internal fluid kinematics numerically, future experimental research is recommended to evaluate the long-term impact of these geometric modifications on mechanical vibrations and cavitation limits under dynamic flow conditions during operation.

Acknowledgments

This research did not receive any specific grant from funding agencies in the public, commercial, or not-for-profit sectors, and all computational analyses were performed utilizing independent, private resources.

References

[1] S. Yang, Z. Wang, W. Zhang, X. Li, and H. Zhang, "Investigate the full characteristic of a centrifugal pump-as-turbine (pat) in turbine and reverse pump modes," *Engineering Applications of Computational Fluid Mechanics*, vol. 17, no. 1, p. 2246527, 2023.

[2] X. Chen, Z. Zhang, J. Huang, X. Zhou, and Z. Zhu, "Numerical investigation on energy change field in a centrifugal pump as turbine under different flow rates," *Renewable Energy*, vol. 230, p. 120804, 2024.

[3] S. Barbarelli, M. Amelio, G. Florio, and N. M. Scornaienchi, "Procedure selecting pumps running as turbines in micro hydro plants," in *Energy Procedia*, vol. 126, pp. 549–556, 2017.

[4] K. Kan, X. Yang, Z. Zhu, X. Li, Y. Lin, and Q. Zhou, "Pump as turbine cavitation performance for both conventional and reverse operating modes: A review," *Renewable and Sustainable Energy Reviews*, vol. 168, p. 112786, 2022.

[5] J. Li, D. Meng, and X. Qiao, "Numerical investigation of flow field and energy loss in a centrifugal pump as turbine," *Shock and Vibration*, vol. 2020, p. 8884385, 2020.

[6] T. Lin, Z. Zhu, X. Li, J. Li, and Y. Lin, "Theoretical, experimental, and numerical methods to predict the best efficiency point of centrifugal pump as turbine," *Renewable Energy*, vol. 168, pp. 31–44, 2021.

[7] H. C. O. Unegbu and D. S. Yawas, "Precision computational modeling of wind flow dynamics to optimize wind turbine deployment in nigeria's varied geographical terrains," *JMES The International Journal of Mechanical Engineering and Sciences*, vol. 10, no. 1, pp. 25–36, 2026.

[8] M. A. Ismail, A. K. Othman, and H. Zen, "Cfd modelling of a pump as turbine (pat) with rounded leading edge impellers for micro hydro systems," in *MATEC Web of Conferences*, vol. 87, p. 05004, 2017.

[9] A. M. Tchada, N. Tchoumboué, A. L. A. Mesquita, and P. Hendrick, "Enhancing pump as turbine (pat) performances: A numerical investigation into the impact of impeller leading edge rounding," *Heliyon*, vol. 10, no. 15, p. e34663, 2024.

[10] S. Saremian and M. H. Shojaeefard, "Study on the impact of volute geometric modification on the performance of centrifugal pump as turbine," *Renewable Energy*, vol. 253, p. 123632, 2025.

[11] T. Lin, X. Li, Z. Zhu, R. Xie, and Y. Lin, "Investigation of flow separation characteristics in a pump as turbines impeller under the best efficiency point condition," *Journal of Fluids Engineering*, vol. 143, no. 6, p. 061204, 2021.

[12] S. V. Jain, A. Swarnkar, K. H. Motwani, and R. N. Patel, "Effects of impeller diameter and rotational speed on performance of pump running in turbine mode," *Energy Conversion and Management*, vol. 89, pp. 808–824, 2015.

[13] A. F. Aulina and H. Hasbiyati, "Aerodynamic performance analysis of tandem savonius wind turbines influenced by lateral gap from adjacent wall," *JMES The International Journal of Mechanical Engineering and Sciences*, vol. 10, no. 1, pp. 1–10, 2026.

[14] A. Nugroho, E. D. Ariyanto, S. R. Ariyanto, L. S. Yuniar, and S.-S. Hsiau, "Enhancing biocrude and hydrochar production from water hyacinth via hydrothermal processing and particle flow analysis," *JMES The International Journal of Mechanical Engineering and Sciences*, vol. 10, no. 1, pp. 45–54, 2026.

[15] A. Imran, U. Ali, and I. Janajreh, "Aerodynamic performance of variable pitch vertical axis wind turbines at low tsr: A transient urans investigation," *Energy Conversion and Management: X*, vol. 30, p. 101857, 2026.

[16] J. Pei, Y. Wang, W. Wang, D. Wang, F. Yang, and W. Shi, "Performance prediction based on effects of wrapping angle of a side channel pump," *Energies*, vol. 12, no. 1, p. 139, 2019.

[17] V. M. Arocena and L. A. M. Danao, "Improving the modeling of pressure pulsation and cavitation prediction in a double-volute double-suction pump using mosaic meshing technology," *Processes*, vol. 11, no. 3, p. 660, 2023.

[18] S. E. Monroe, J. Wang, and C. Liang, "Performance studies of an axial flow waterjet pump using an unsteady reynolds-averaged navier–stokes model," *New England Journal of Computational Science*, vol. 6, no. 1, 2024.

[19] D.-Y. Li, L. Han, H.-J. Wang, R.-Z. Gong, X.-Z. Wei, and D.-Q. Qin, "Pressure fluctuation prediction in pump mode using large eddy simulation and unsteady reynolds-averaged navier–stokes in a pump–turbine," *Advances in Mechanical Engineering*, vol. 8, no. 6, p. 1687814016652562, 2016.

[20] P. Neittaanmäki, T. Rossi, K. Majava, O. Pironneau, W. Rodi, and M. Strelets, "On urans solutions with les-like behaviour," in *Proceedings of ECCOMAS CFD*, 2004. Available online: https://api.semanticscholar.org/CorpusID:126147486.

[21] A. Nasir, E. Dribssa, M. Girma, and H. B. Madessa, "Selection and performance prediction of a pump as a turbine for power generation applications," *Energies*, vol. 16, no. 13, p. 5036, 2023.

[22] Y.-I. Kim, H.-M. Yang, K.-Y. Lee, and Y.-S. Choi, "Influence of blade leading edge shape on hydraulic and suction performance of a mixed-flow pump," *Journal of Physics: Conference Series*, vol. 2217, no. 1, p. 012048, 2022.

[23] H. Luo, R. Tao, J. Yang, and Z. Wang, "Influence of blade leading-edge shape on rotating-stalled flow characteristics in a centrifugal pump impeller," *Applied Sciences*, vol. 10, no. 16, p. 5635, 2020.

[24] R. Tao, R. Xiao, and Z. Wang, "Influence of blade leading-edge shape on cavitation in a centrifugal pump impeller," *Energies*, vol. 11, no. 10, p. 2588, 2018.

[25] G. Shi, Z. Liu, Y. Xiao, H. Li, and X. Liu, "Tip leakage vortex trajectory and dynamics in a multiphase pump at off-design condition," *Renewable Energy*, vol. 150, pp. 703–711, 2020.